THE ASTROPHYSICAL JOURNAL, 429:602–611, 1994 July 10

EXTENDED INFRARED LINE EMISSION EXCITED BY STARBURST AND SEYFERT ACTIVITY IN NGC 3256 AND NGC 4945[1]

A. F. M. MOORWOOD
European Southern Observatory, Karl Schwarzschild Strasse 2, D-85748 Garching, Germany
AND
E. OLIVA
Osservatorio Astrofisico di Arcetri, Largo E. Fermi 5, I-50125, Firenze, Italy
Received 1993 June 29; accepted 1994 January 10

ABSTRACT

We present visible and infrared images, 1.5–2.3 μm infrared spectra and [Fe II] 1.64 μm, H_2 (1–0)S(1) 2.121 μm, and Brγ 2.165 μm infrared line contour maps obtained to investigate the nature of the activity and the origin of the infrared line emission in two relatively nearby infrared luminous galaxies. NGC 3256 is a merging system exhibiting starburst activity over a region several kpc across and a high infrared luminosity of $\sim 3 \times 10^{11}\ L_\odot$. A specific search for [Si VI] 1.96 μm coronal line emission from a possibly visually obscured Seyfert nucleus proved negative. Extremely high star-formation and SN rates of $\sim 20\ M_\odot\ \mathrm{yr}^{-1}$ and $\sim 1.5\ \mathrm{yr}^{-1}$, respectively, however, are estimated using the observed integrated Brγ line luminosities and He I 2.06 μm/Brγ ratios together with an existing starburst model. At this rate, the injection energy associated with SN explosions alone could account for the observed [Fe II] 1.64 μm and H_2 (1–0)S(1) line luminosities. NGC 4945 is an almost edge-on spiral with an order of magnitude lower infrared luminosity which is powered by both a $\sim$400 pc size starburst and a visually obscured Seyfert nucleus which is a variable source of hard X-ray emission and could substantially contribute to the total luminosity. Its star formation efficiency is higher than in NGC 3256 whereas its luminosity and star formation and SN rates of $\sim 0.4\ M_\odot\ \mathrm{yr}^{-1}$ and $\sim 0.05\ \mathrm{yr}^{-1}$ are much lower although still adequate to account for the excitation of the observed [Fe II] 1.64 μm and H_2 (1–0)S(1) lines. Based on previous survey work, however, the large integrated H_2 (1–0)S(1)/Brγ ratio observed in this galaxy is also indicative of the presence of a Seyfert nucleus. Maps of the Brγ, [Fe II], and H_2 (1–0)S(1) line emission reveal significantly different spatial distributions in the two galaxies. In NGC 3256 the emission extends over a region $\sim$4 kpc across and shows similar [Fe II] and Brγ morphologies, whereas the H_2 (1–0)S(1) emission does not correlate in detail with either. In particular, it is less peaked on the nucleus and traces a spiral arm and embedded source to the south of the nucleus. This source is also prominent in our K' (2.1 μm) image but totally obscured by dust in the visible and is probably the nucleus of the merging companion. Additional evidence that the merger is not yet complete is also provided by the fact that the light distribution in the K' image does not correspond to that expected of a relaxed system. In NGC 4945 the Brγ emission is largely confined to a $\sim$380 pc diameter and $\leq$190 pc thick disk in the plane of the galaxy whereas both the [Fe II] 1.64 μm and H_2 (1–0)S(1) line emission extends over the full extent of the molecular complex which is a factor of 2 larger perpendicular to the plane. This morphology is consistent with additional excitation by an embedded active galactic nucleus and/or a starburst driven superwind. The similarity of the observed [Fe II] and H_2 intensity profiles perpendicular to the plane suggests a common excitation mechanism for the "excess" emission which we propose can be attributed to partial ionization and heating of molecular gas respectively by X-rays from the nuclear source. The overall conclusion of this study is that NGC 4945 is probably at an advanced stage of its evolution from a starburst to a Seyfert galaxy whereas there is no evidence that such an evolution is occurring yet in the considerably more luminous, merging system, NGC 3256.

Subject headings: galaxies: individual (NGC 3256, 4945) — galaxies: interactions — galaxies: ISM — galaxies: Seyfert — galaxies: starburst — infrared: galaxies

1. INTRODUCTION

NGC 3256 and NGC 4945 are interesting examples of infrared luminous galaxies harboring massive molecular complexes which are close enough for detailed observations relevant to our understanding of the nature and possible evolution of their nuclear activity. NGC 3256 is a highly luminous merging system which appears to be powered exclusively by starburst activity whereas NGC 4945, although an order of magnitude less luminous, exhibits both starburst and Seyfert characteristics. We have chosen to discuss these two galaxies together, therefore, in relation to the long standing question as to whether or not Seyfert activity can be attributed to the presence of supermassive objects formed from the collapsed remnants of nuclear starbursts (e.g., Weedman et al. 1981; Krügel, Tutukov, & Loose 1983). The luminosity of NGC 3256 is also within a factor of 2–3 of the so-called Ultraluminous Infrared Galaxies (UIGs), detected by *IRAS*, which Sanders et al. (1988) have proposed may contain visually obscured quasars formed following merger induced starbursts although conclusive evidence for the presence of active galactic nucleus (AGN) activity

[1] Based on observations collected at the European Southern Observatory, La Silla, Chile.

has so far proved elusive (Rieke 1988; Allen et al. 1991; Condon et al. 1991; Lonsdale, Lonsdale, & Smith 1992).

The main aim of the present study was to follow up our earlier infrared spectroscopic observations of these galaxies by mapping the Brγ (2.167 μm), [Fe II] (1.64 μm) and H_2 (1–0)S(1) (2.121 μm) line emission to delineate any extended photoionized, shock, and UV/X-ray heated circumnuclear gas, respectively (cf. Moorwood & Oliva 1993a, b) e.g., to test for the presence of SN-driven winds which may produce shock excited LINER type optical spectra (cf. Heckman, Armus, & Miley 1990) as actually observed in most of the UIGs and could be the controlling factor in the evolution of starbursts (Krügel et al. 1983). Additional spectra were also obtained around the [Si VI] (1.96 μm) coronal line, to test specifically for the presence of Seyfert activity (Oliva & Moorwood 1990; Moorwood & Oliva 1993a, b), and other [Fe II] and H_2 lines plus He I (2.058 μm) which can provide further constraints on the physical conditions and stellar content in the circumnuclear regions. Optical and near-infrared images were also obtained to search for visually obscured sources and to investigate further the controversial question as to whether or not NGC 3256 is already a fully merged system.

1.1. *NGC 3256*

NGC 3256 is a merging system exhibiting the double tidal tails characteristic of an interaction between two spiral galaxies of comparable mass (de Vaucouleurs & de Vaucouleurs 1961; Toomre & Toomre 1972). Optical images of the central region show a prominent nucleus, several "hot spots," and obvious evidence of large and patchy extinction but no obvious candidate for the nucleus of the merging companion except, possibly, a bright structure $\sim$10″ SW of the nucleus (Lauberts et al. 1978). Optical spectra reveal a complex velocity structure and a possible displacement of the minor axis about 1 kpc to the west of the nucleus (Feast & Robertson 1978). Whereas Schweizer (1983, 1986) has not classified it as a complete merger, on morphological grounds, Graham et al. (1984, 1987) have proposed that it is already a relaxed system which will appear as an elliptical galaxy once the residual gas has been blown out by supernova-driven winds associated with its prominent starburst activity. Heckman et al. (1990) include it in their sample of galaxies having possible starburst-driven winds although it is not discussed in detail and there appears to be no specific evidence for one e.g., line splitting as found in NGC 4945. Its near-infrared colors from J, H, K, L band photometry are indicative of a young starburst (Glass & Moorwood 1985) and near-infrared spectra show [Fe II] and H_2 emission lines (Moorwood & Oliva 1988, 1990) and a prominent 3.28 μm feature with an equivalent width typical for starburst galaxies (Moorwood 1986). Assuming $H_0 = 50$ km s^{-1} Mpc^{-1} its infrared luminosity derived from *IRAS* data is $\sim 6 \times 10^{11}$ $L_\odot$ (only a factor of 2 lower than the so-called Ultraluminous Infrared Galaxies) which, based on its energy distribution, can be mostly attributed to the starburst (Rowan-Robinson & Crawford 1989). At the nearer distance of 37 Mpc adopted here (Graham et al. 1984) its infrared luminosity is only $\sim 3 \times 10^{11}$ $L_\odot$ but still an order of magnitude higher than that of the well studied starburst galaxy M82. Extended 10 μm emission which is also, presumably, associated with the starburst extends over a region several kpc across with most originating outside the central 1 kpc (Graham et al. 1987). A central molecular complex mapped in CO extends over $\sim$12 kpc and contains an estimated 3×10^{10} $M_\odot$ of molecular hydrogen which is amongst the highest found in any galaxy and half of which is located outside the central 2.5 kpc (Sargent, Sanders, & Phillips 1989).

1.2. *NGC 4945*

NGC 4945 is an almost edge-on ($i \sim 80°$) spiral galaxy of angular size $\sim 17' \times 3'$ which has been classified as SB by de Vaucouleurs, de Vaucouleurs & Corwin (1976) and whose visible appearance is dominated by a prominent dust lane which obscures the actual nucleus. It is probably a member of the Centaurus group now generally believed to be at a distance of $\sim$3.9 Mpc (cf Bergman et al. 1992) which we shall assume here. At this adopted distance its total infrared luminosity derived from the *IRAS* survey data is $\sim 2.7 \times 10^{10}$ $L_\odot$ (Rice et al. 1988) of which, based on independent airborne observations, $\sim 2 \times 10^{10}$ $L_\odot$ arises from a region of only 12″ × 9″ centered on the nucleus (Brock et al. 1988) which is somewhat smaller than the central 33″ × 19″ (640 × 340 pc) molecular complex mapped in CO (Whiteoak et al. 1990; Bergman et al. 1992). The nucleus itself is a strong radio continuum source emitting 2 Jy at 6 GHz (Whiteoak & Wilson 1990) and one of the first H_2O and OH megamaser sources detected (dos Santos & Lepine 1979; Baan 1985). Although its infrared energy distribution, including prominent 3.28 μm emission and 9.7 μm absorption features, is characteristic of starburst activity, evidence of hot dust or nonthermal near infrared emission and large [N II] (0.6583 μm)/Hα line ratios near to the nucleus could reflect the presence of a Seyfert nucleus (Moorwood & Glass 1984). These authors have also speculated that this galaxy may be in the phase of evolving from a starburster to a Seyfert predicted by the repetitive starburst model of Krügel et al. (1983). Some of the optical line emission has, alternatively, been attributed to shock excitation by a starburst-driven superwind at the surface of a cone or bubble by Heckman et al. (1990) who have observed line splitting of 300–600 km s^{-1} at distances of 70–700 pc from the nucleus. Additional evidence for outflow is provided by the polarization of the extranuclear radio emission (Harnett et al. 1989); radial velocity components in the CO emission (Whiteoak et al. 1990) and the morphology of the optical filaments (Nakai 1989). Near-infrared spectra of the nucleus also show prominent [Fe II] and H_2 emission lines and a large H_2 (1–0)S(1)/Brγ ratio characteristic of composite starburst/Seyfert galaxies (Moorwood & Oliva 1988) which was tentatively attributed by Moorwood & Oliva (1989) to shock heating by an AGN-driven wind. The presence of a Seyfert nucleus now appears to have been definitively confirmed by the recent detection of hard X-rays which are variable on a timescale of hours (Iwasawa et al. 1993).

2. OBSERVATIONS

The infrared spectra and line maps presented here were obtained in 1992 January and 1993 April using the long-slit infrared grating spectrometer IRSPEC at the 3.5 m ESO NTT telescope. This spectrometer is equipped with a 58 × 62 element SBRC InSb array detector whose pixels subtend 2.″2 on the sky (Moorwood, Moneti, & Gredel 1991). The effective slit length is $\sim$100″ and 1 pixel corresponds to 95 km s^{-1} at the wavelength of the [Fe II] 1.64 μm line and 65 km s^{-1} at H_2 2.12 μm and Brγ 2.17 μm. For both galaxies the slit was oriented NE-SW. Each of the spectral lines was measured by setting the grating to the appropriate redshifted center wavelength and making alternate integrations of typically 1 minutes with

the 2".2 slit on and off the galaxy. Two-dimensional line maps were made by repeating this procedure with the slit at a number of positions separated by 2".5 along a line perpendicular to the slit. By making use of OH sky lines (Oliva & Origlia 1992) observed in the same frames the final wavelength accuracy achieved corresponds to ~0.3 pixel. Spectra were flat-fielded by dividing by measurements of an integrating sphere illuminated by a continuum halogen lamp provided for this purpose and flux calibrated using observations of standard stars. Line and continuum maps were then finally constructed from these spectra using a set of programs and procedures written by one of us (E.O) which are now available under CONTEXT/IRSPEC in the ESO MIDAS data reduction package.

Additional long-slit spectra covering [Fe II] (1.536, 1.60, and 1.64 μm); H_2 (1–0)S(3) 1.957 μm; [Si VI] (1.962 μm); He I(2.058 μm); H_2 (1–0)S(1) 2.121 μm and (2–1)S(1) 2.247 μm and Brγ (2.166 μm) were made in a similar way but with a 4".4 wide slit centered only on the nucleus.

Broad-band infrared images of both galaxies were made in 1992 May at the ESO/MPIA 2.2 m telescope using the new IRAC2 camera equipped with a 256 × 256 Rockwell NICMOS3 array (Moorwood et al. 1992). NGC 4945 was observed in the J(1.25 μm) and K(2.2 μm) bands using the 0".49 pixel^{-1} scale and NGC 3256 in K'(2.1 μm) using both the 0".49 and 0".27 pixel^{-1} scales.

An R band CCD image was obtained of NGC 4945 in 1991 April using EMMI (ESO Multi-Mode Instrument) at the NTT and an Hα image of NGC 3256 in 1993 April using SUSI (Superb Seeing Imager) at the NTT.

3. RESULTS

3.1. *Infrared Spectra*

Figure 1 shows composites of the infrared spectra covering various emission lines of interest obtained on the nuclei of NGC 3256 and NGC 4945. None of the detected lines are clearly resolved at our two-pixel resolutions of 190 km s^{-1} at 1.6 μm and 130 km s^{-1} around 2 μm. Both galaxies show prominent He I 2.058 μm emission indicative of the presence of hot stars while the [Si VI] 1.96 μm coronal line associated with Seyfert activity is not detected in either galaxy. Line ratios obtained from these spectra and used in the later discussion are given in Table 1.

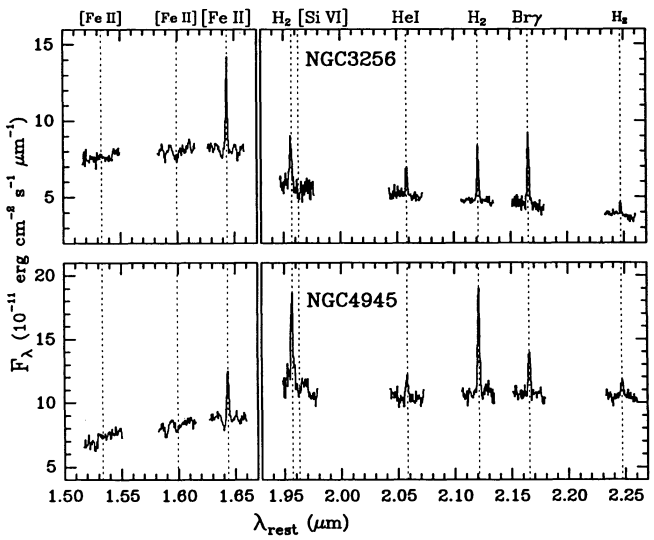

FIG. 1.—Infrared spectra of NGC 3256 and NGC 4945 covering specific emission lines of interest. The effective apertures are 4".4 × 11" and 4".4 × 15", respectively, centered on the nucleus in each case.

3.2. *Images and Maps*

3.2.1. *NGC 3256*

Figure 2 (Plate 5) shows our K'(2.1 μm) and narrow-band Hα (+continuum) images of NGC 3256. The K' image is dominated by a central peak (nucleus) whose FWHM is 1".6 in both the NS and EW directions. To the E are two much fainter peaks which coincide in position with the two relatively more prominent "hot spots" in the visible image. About 5" S of the nucleus is a brighter (~10% of the nucleus) K' source whose position is marked by the cross on the visible image where it has no counterpart due to high extinction in this region. This source appears to be embedded in a spiral arm which originates in the nucleus and becomes visible also in the optical to the W. There is diffuse emission to the SW in both images but no obvious peak at the position suggested by Lauberts et al. (1978) for the merging companion. Recent radio observations have also revealed a double source with peaks of comparable brightness on the "nucleus" and our K' source to the S (Norris & Forbes 1994). Given that some of the difference in their K' brightness may be due to extinction, therefore, we conclude that this peak to the S is most probably the nucleus of the merging companion. This would support the argument of Schweizer (1983, 1986), based on its more general morphology, that the merger is not yet complete but conflicts with the conclusion of Graham et al. (1984) that the light distribution over the central 5 kpc, as deduced from multiaperture K band photometry, is already consistent with the $r^{1/4}$ profile characteristic of a relaxed system. As shown in Figure 3, however, the higher resolution profile over the central 15 kpc obtained by averaging over ellipses fitted to our K' image is clearly not that of a relaxed elliptical galaxy. It is of interest also that the fitted ellipses indicate a minor axis tilted roughly 18°. NW in the plane of the sky and ~30° to the line of sight. While this tilt to the line of sight is in reasonable agreement with the ~40° deduced by Feast & Robertson (1978) from contours further out the tilt in the plane of the sky conflicts with the ~20°. NE deduced from their detailed spectroscopic study of the kinematics.

Figure 4 (Plate 6) shows the [Fe II] 1.64 μm, H_2 (1–0)S(1) 2.121 μm and Brγ 2.165 μm line maps made with IRSPEC superposed on the K' band image for reference. Registration of the line maps with the image was achieved via maps of the continuum under the lines produced from the same IRSPEC spectra. In all cases the contour levels are 1, 0.75, 0.5,

TABLE 1

INFRARED LINE RATIOS

Ratio	NGC 4945 (4".4 × 11")	NGC 3256 (4".4 × 15")
[Fe II] 1.53 μm/[Fe II] 1.64 μm	<0.1	<0.1
[Fe II] 1.60 μm/[Fe II] 1.64 μm	<0.1	<0.1
[Si VI] 1.96 μm /H_2 (1–0)S(3)	<0.1	<0.2
He I 2.06 μm/Brγ 2.165 μm	0.62 ± 0.18	0.48 ± 0.07
H_2 (1–0)S(1)/Brγ 2.165 μm	2.53 ± 0.4	0.82 ± 0.11
H_2 (1–0)S(1)/[Fe II] 1.64 μm	1.82 ± 0.26	0.53 ± 0.07
H_2 (2–1)S(1)/H_2 (1–0)S(1)	0.13 ± 0.03	0.13 ± 0.03
[Fe II] 1.64 μm/Brγ 2.165 μm	1.4 ± 0.2	1.55 ± 0.2

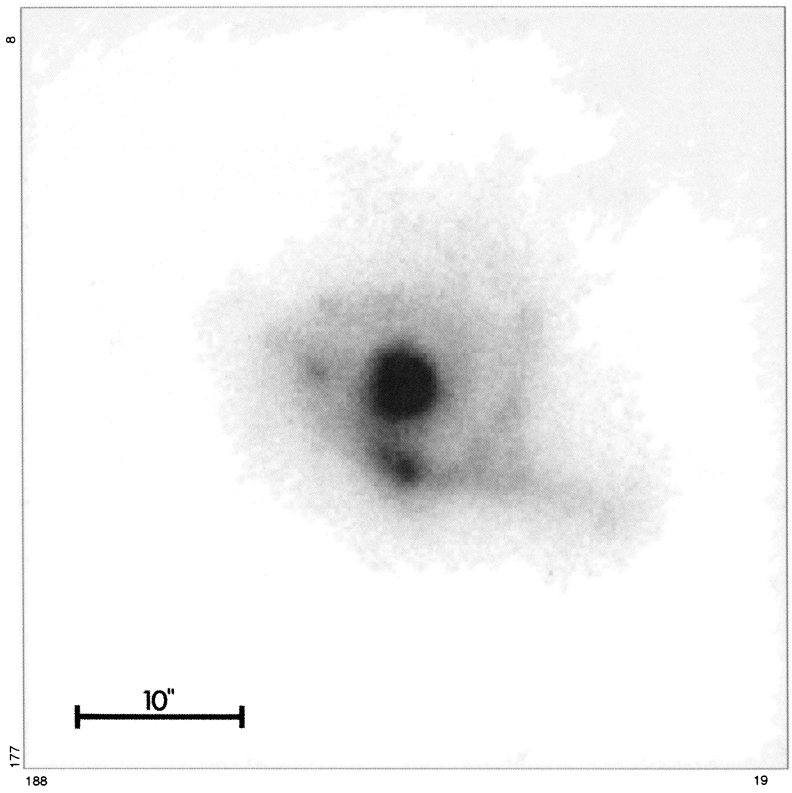

FIG. 2a

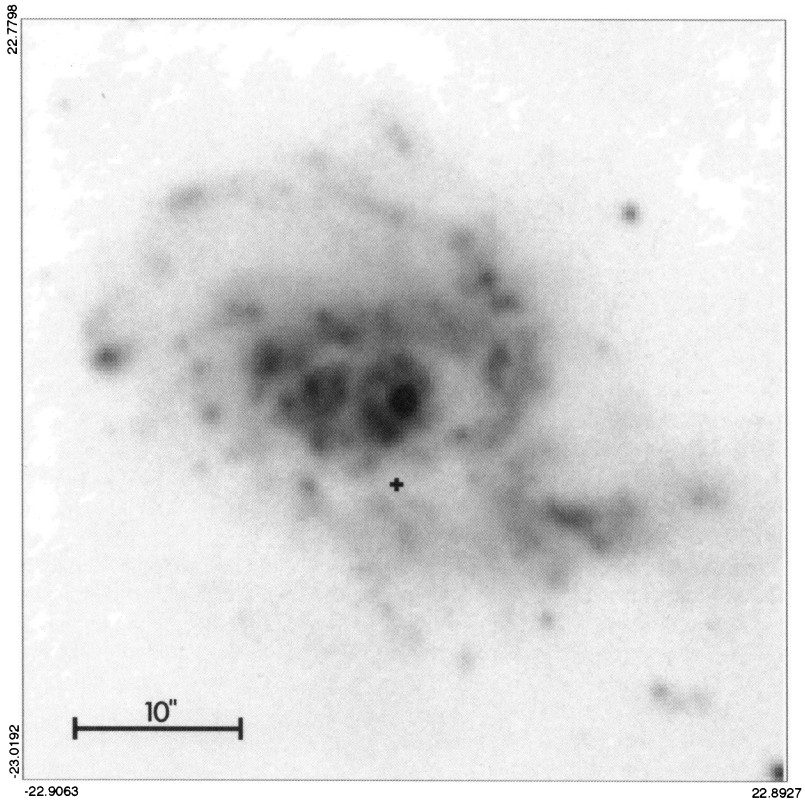

FIG. 2b

FIG. 2.—Images of NGC 3256. (*a*) K'(2.1 μm); (*b*) Hα (+continuum). N is at the top and E is to the left and the scale bars are 10″. The cross on the Hα image marks the position of the visually obscured K' source to the S of the nucleus.

PLATE 6

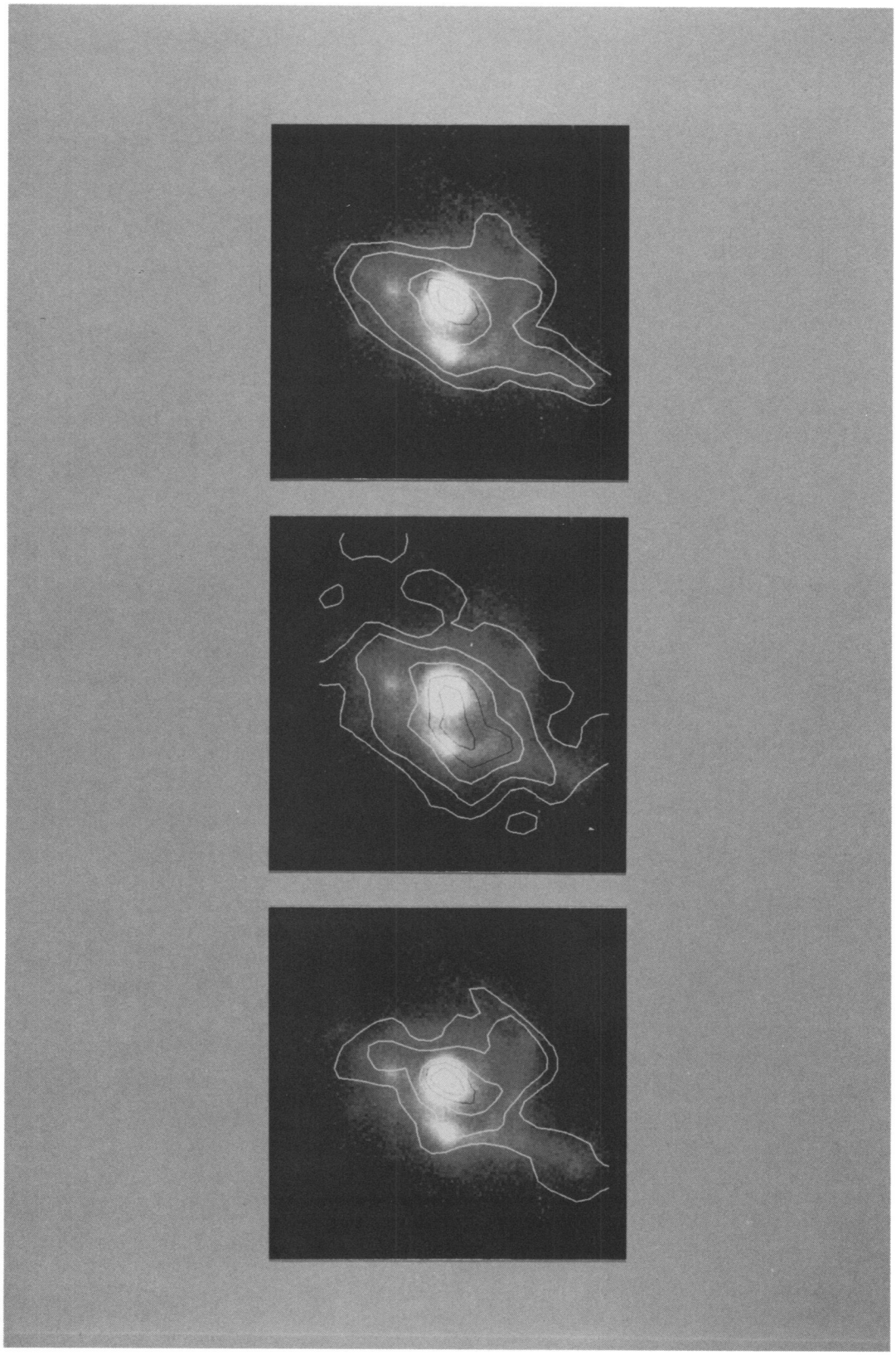

FIG. 4.—Infrared emission line contour maps superposed on the K' image of NGC 3256. N is at the top and E is to the left and the field is 34″ × 34″. *Upper panel*: [Fe II] 1.64 μm, *middle panel*: H_2 (1–0)S(1) 2.121 μm, *bottom panel*: Brγ 2.17 μm. The contour levels are 1, 0.75, 0.5, 0.25, and 0.12 normalized to the peak surface brightness in each case.

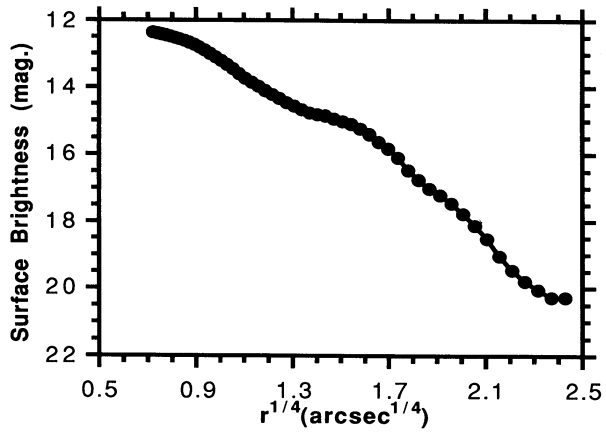

FIG. 3.—Surface brightness vs. $r^{1/4}$ derived by averaging over ellipses fitted to the K' image of NGC 3256.

0.25, and 0.12 normalized to the peak surface brightness in order to provide the same dynamic range in each map and the lowest contours have signal-to-noise ratios corresponding to $\sim 4\ \sigma$, $2\ \sigma$, and $3\ \sigma$, respectively. Integrated fluxes, extinction corrected luminosities and approximate sizes of the line emitting regions are reported in Table 2. The line emission is extended over a region ~ 4 kpc and shows a morphology which is superficially similar to the 10 μm emission mapped by Graham et al. (1987) but with some obvious detailed differences in the spatial distribution of the three lines. Brγ peaks strongly on the nucleus but is also associated with the sources to the E and S, which are not resolved due to the lower spatial resolution of IRSPEC, and the diffuse optical emission to the SW and NW. The [Fe II] distribution is superficially similar to that of Brγ but is less peaked at the positions of the visible/K' sources and extends slightly further to the S-SE. The H_2 emission is somewhat more extended than the other lines, particularly again to the S-SE and its detailed spatial distribution is not well correlated with either. In the central region it is less strongly peaked on the nucleus and actually exhibits the same surface brightness on the source to the S where its ratio with both Brγ and [Fe II] is a factor of three larger than on the nucleus. It also traces the southern spiral arm, which is not really evident in the other maps, whereas it shows no peak corresponding to the Brγ/Hα sources to the E and is less pronounced than the other lines to the NW.

The extension of both the [Fe II] and H_2 emission relative to Brγ in the S-SE is in the approximate direction we find for the minor axis and therefore could result from projection effects if the emission in these lines extends further out of the plane.

Figure 5 (Plate 7) shows Brγ line contours corresponding to 65 km s^{-1} wide velocity bins centered at 2700 and 2950 km s^{-1} on either side of the systemic velocity overlaid on the K' image. This "snapshot" illustrates the complex dynamics of the system which does not appear to have a single rotational axis. If the emission to the NW (which is associated with an H II complex in the Hα image) is ignored, however, the implied rotational axis is inclined $\sim 25°$ to the NW in reasonable agreement with the position deduced by fitting ellipses to the K' image.

3.2.2. *NGC 4945*

Figure 6 (Plate 8) is our J (1.25 μm) band image of NGC 4945 and Figure 7 shows R, J, and K(2.2 μm) contour maps and images of the nuclear region. Both the R and J images show "fan"-shaped emission and the prominent dust lane which visually obscures the nucleus whose position, as determined from the K band image, is marked with a cross on the R image. Some additional detail on the nucleus is present in the J image compared with an earlier one already presented elsewhere (Moorwood & Origlia 1990). Whereas the FWHM along the major axis is 3".2 the emission along the minor axis shows additional peaks and is more extended with a FWHM of $\sim 6''.5$. At K the nucleus has the same FWHM of 3".2 observed at J along the major axis but only 1".8 along the minor axis. As the position of peak J flux corresponds to the center of the K band emission it is possible that the additional extension in this and the R band is due to dust scattering of radiation from the nuclear source.

Figure 8 (Plate 9) shows the [Fe II] 1.64 μm, H_2 (1–0)S(1) 2.121 μm and Brγ 2.165 μm line maps obtained with IRSPEC superposed on the J band image as a reference. Registration of the line maps with the image was achieved via maps of the continuum under the lines produced from the same IRSPEC spectra. In all cases the contour levels in the maps are again 1, 0.75, 0.5, 0.25, 0.12 normalized to the peak surface brightness in

TABLE 2

INTEGRATED PROPERTIES FROM LINE MAPS

Quantity	[Fe II] 1.64 μm	H_2 2.12 μm	Brγ 2.17 μm
NGC 3256			
Observed flux in map (10^{-20} W cm^{-2})	2.4	1.1	1.5
Extinction (mag)[a]	0.22	0.14	0.13
Dereddened luminosity (L_0) in map	1E7	4.3E6	5.7E6
Extent	27" × 16"	19" × 13"	26" × 13"
Extent (pc)	4450 × 2640	3130 × 2140	4290 × 2140
NGC 4945			
Observed flux in map (10^{-20} W cm^{-2})	1.2	3.1	0.97
Extinction (mag)[b]	1.8	1.12	1.08
Dereddened luminosity (L_0) in map	3E5	4E5	1.2E5
Extent	18" × 21"	20" × 20"	20" × 10"
Extent (pc)	340 × 400	380 × 380	380 × 190

[a] From Pβ/Brγ = 4.9 assuming intrinsic ratio = 5.9 and $\tau\alpha\lambda^{-1.85}$.

[b] From Brα/Brγ = 5.6 (Moorwood & Oliva 1988) assuming intrinsic ratio = 2.83 and $\tau\alpha\lambda^{-1.85}$ (Landini et al. 1984).

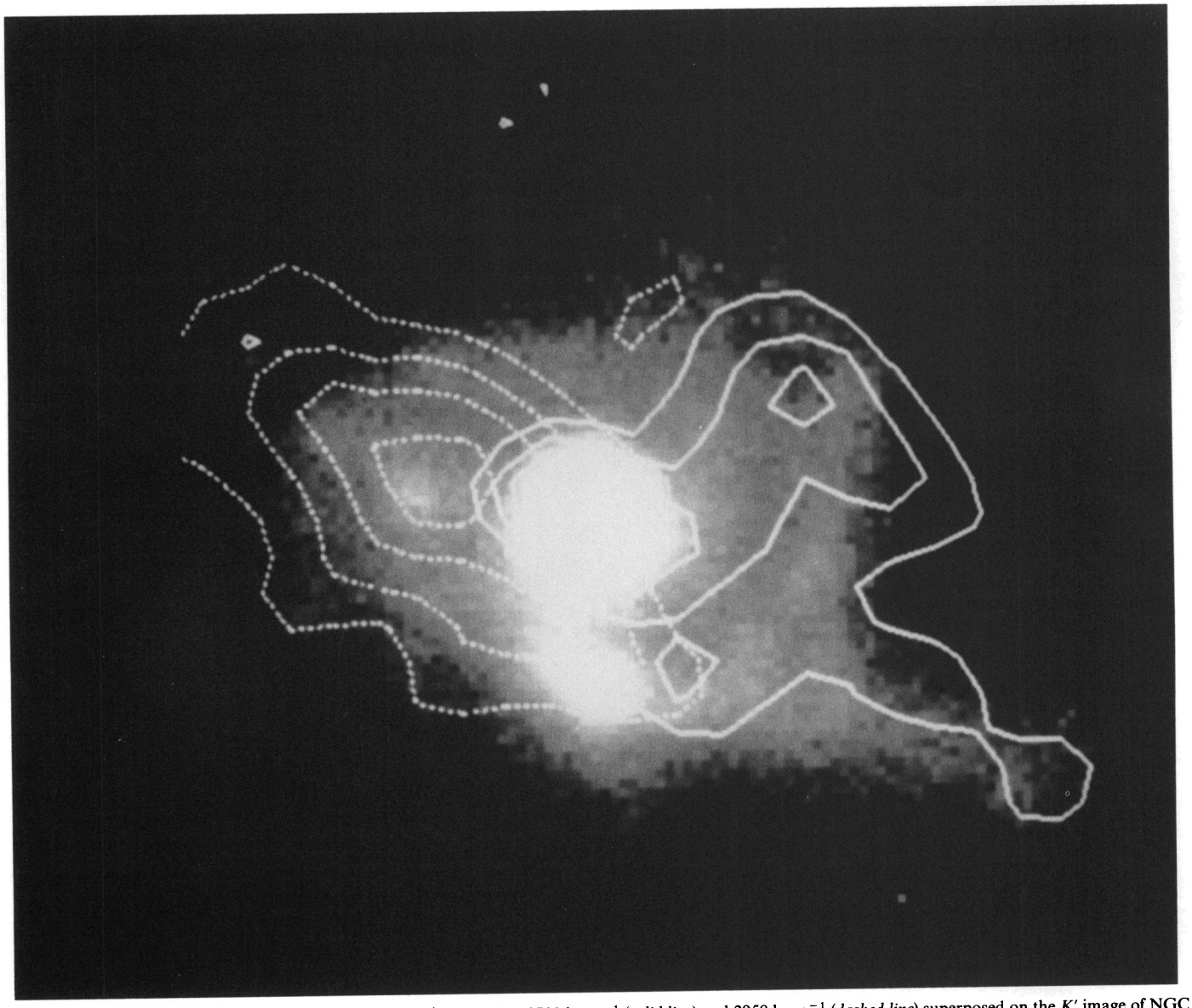

FIG. 5.—Brγ line contours for velocity bins of 65 km s^{-1} centered at 2700 km s^{-1} (*solid line*) and 2950 km s^{-1} (*dashed line*) superposed on the K' image of NGC 3256. N is at the top and E is to the left and the field is 36″ × 31″.

MOORWOOD & OLIVA (see 429, 605)

PLATE 8

FIG. 6.—*J* (1.25 μm) band image of NGC 4945. The image scale is 0.″5 pixel^{-1} and the field is 127″ × 84″ with N at the top and E is to the left. A prominent nucleus is just visible at the edge of the dust lane in the plane of the galaxy which is approximately aligned with the major axis.

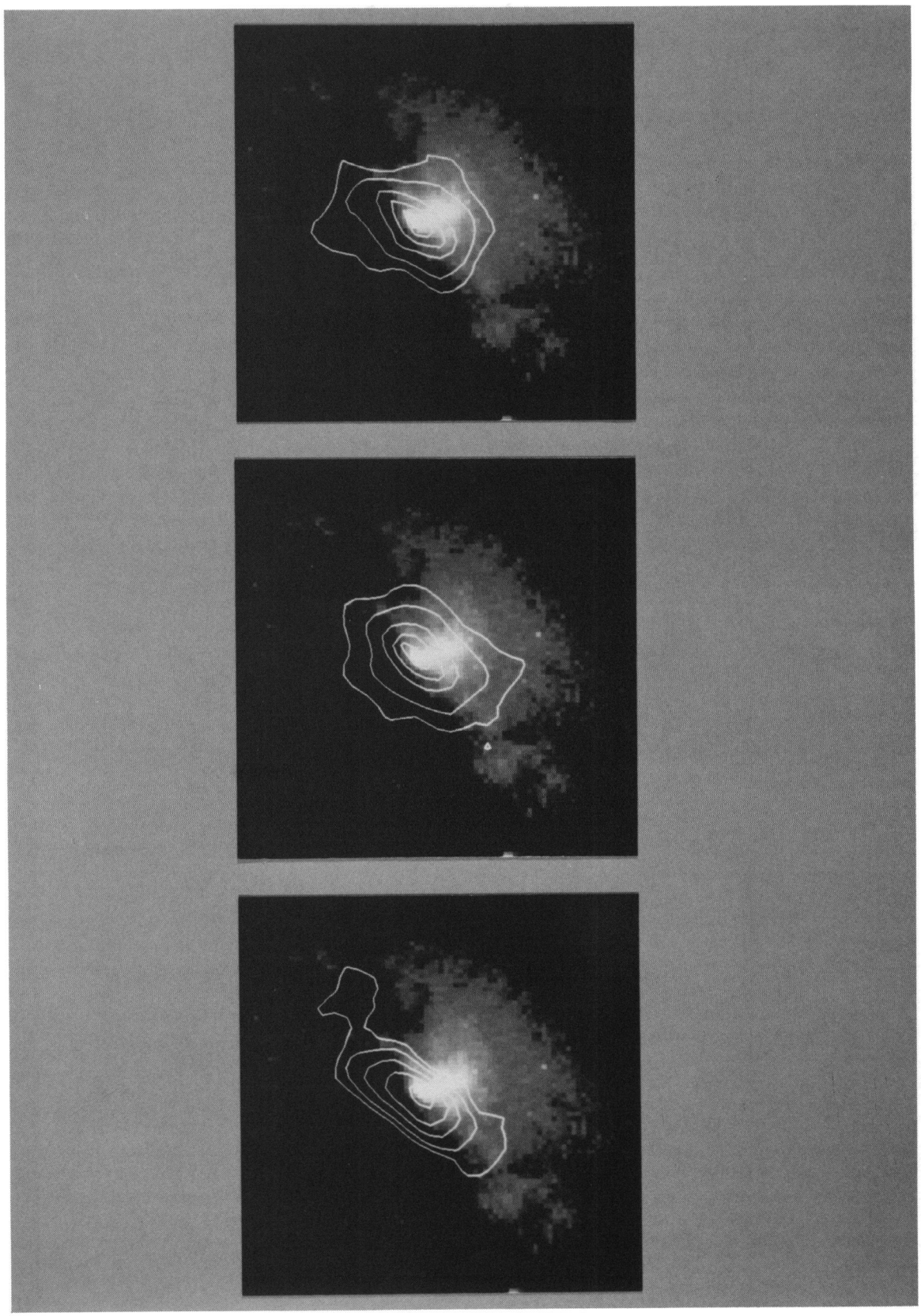

FIG. 8.—Infrared emission line contour maps superposed on the *J* band image of NGC 4945. N is at the top and E is to the left and the field is 41″ × 41″. *Upper panel*: [Fe II] 1.64 μm; *middle panel*: H_2 (1–0)*S*(1) 2.121 μm; *bottom panel*: Brγ 2.17 μm. The contour levels are 1, 0.75, 0.5, 0.25, and 0.12 normalized to the peak surface brightness in each case.

MOORWOOD & OLIVIA (see 429, 605)

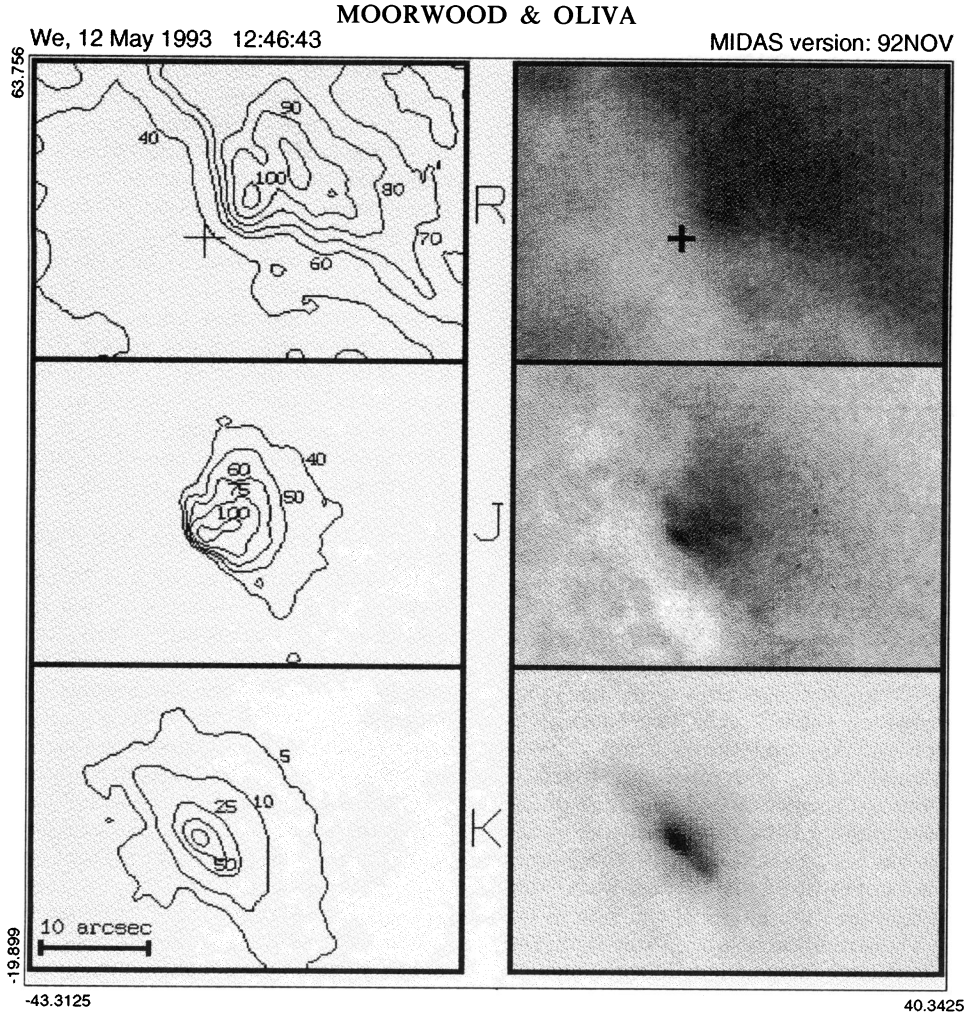

FIG. 7.—*R*, *J*, and *K* (2.2 μm) band images and contour maps of the nuclear region in NGC 4945. The cross on the *R* band image marks the position of the nucleus measured at *K*.

order to provide the same dynamic range in each map and the lowest contours have signal-to-noise ratios corresponding to 4 σ, 6 σ, and 4 σ, respectively. Integrated line fluxes and extinction corrected luminosities together with the approximate sizes of the line emitting regions are given in Table 2. In this case the differences in spatial distribution are considerably more obvious than in NGC 3256. Apart from the source to the NE, which is probably an extranuclear H II region, the observed Brγ spatial distribution is consistent with its being confined to a disk of diameter $\sim$380 pc and thickness $\lesssim$190 pc in the plane of the galaxy. In contrast, the H_2 and [Fe II] emission, although comparable in extent along the major axis, is more extended by a factor of 2 in the perpendicular direction where it is present out to the limits of the molecular complex mapped in CO. As both these lines peak on the nucleus it also appears more likely that they originate in the thick ($\sim$350 pc) disk favored by Whiteoak et al. (1990) than a molecular ring as proposed by Bergman et al. (1992) on the basis of CO data. The [Fe II] map also shows no evidence for the dust extinction which is clearly visible both in the map of the continuum under this line and in the *J* band image.

The lines are unresolved in all spectra and no line splitting is observed at any position within the region mapped. Figure 9 (Plate 10) shows H_2 line contours for velocity slices 65 km s^{-1} wide centered at 460 (*solid line*) and 730 (*dashed line*) km s^{-1} superposed on the *J* image which reveal a much simpler dynamical situation than in NGC 3256 with a clearly defined rotational axis aligned roughly perpendicular to the dust lane. Figure 10 shows the rotation curves derived from the H_2 and Brγ lines measured along the major axis. Both curves are similar and yield the same velocity gradient of $\sim$15 km s^{-1} arcsec^{-1} across the central region as derived from CO observations by Whiteoak et al. (1990). The implied total mass is $\sim 3 \times 10^8\ M_\odot$ within the central 18″ or $\sim 10^9\ M_\odot$ within the central 30″. Compared with the CO observations our maps have much higher spatial resolution but inferior velocity resolution. It is of interest to note therefore that the small "bumps" in the H_2 curve at $\sim \pm 6''$ correspond closely in position with and hence provide independent evidence for the presence of the inner rotating ring deduced from common pairs of CO velocity features by Whiteoak et al. (1990). The fact that the systemic velocity of 560 km s^{-1} occurs close to the nucleus, however, argues against the 5″ displacement of the rotational axis tentatively claimed by these authors.

4. DISCUSSION

4.1. *NGC 3256*

4.1.1. *Starburst Properties*

Although clearly a merging system in which massive star formation is occurring over an extended region the integrated properties of NGC 3256 are remarkably similar to the well

PLATE 10

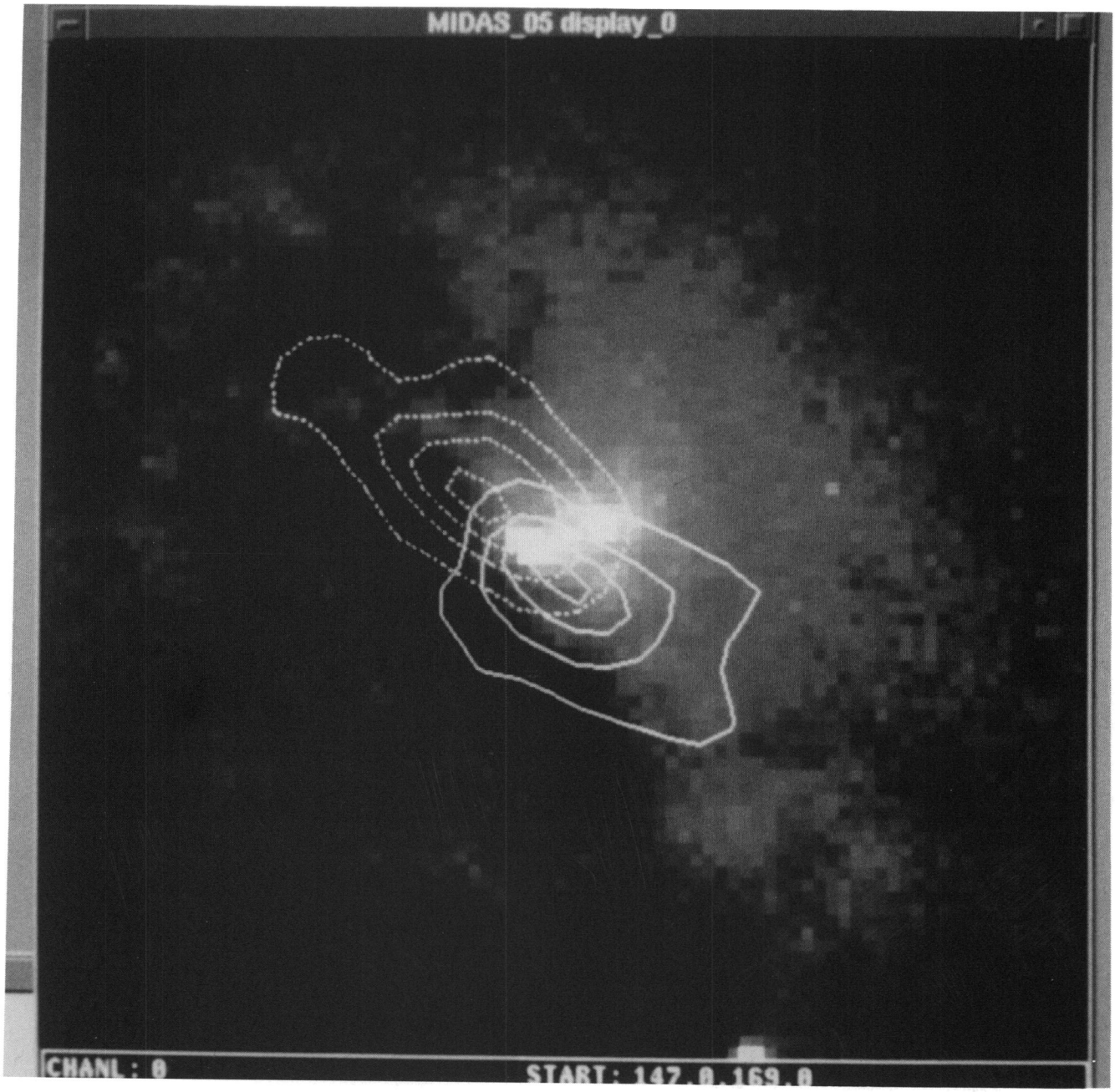

FIG. 9.—H_2 (1–0)S(1) line contours for velocity bins of 65 km s^{-1} centered at 460 km s^{-1} (*solid line*) and 730 km s^{-1} (*dashed line*) superposed on the J image of NGC 4945. N is at the top and E is to the left and the field is 43″ × 41″.

MOORWOOD & OLIVA (see 429, 606)

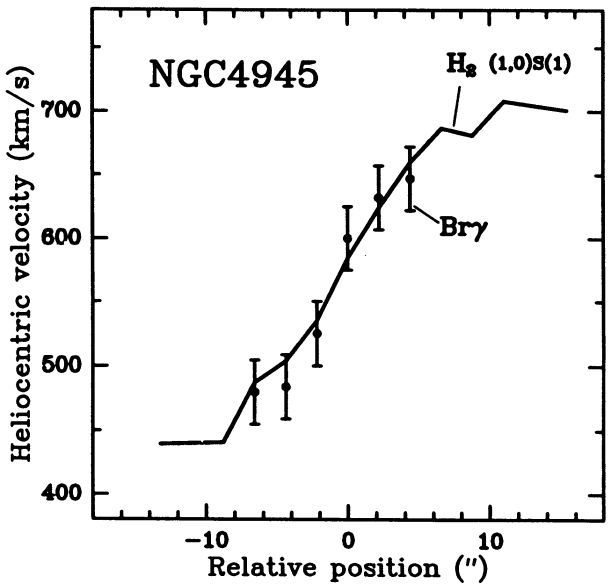

FIG. 10.—Rotation curves along the major axis of NGC 4945 for H_2 (1–0)$S(1)$ (*solid line*) and Brγ (*points*).

studied starburst galaxy M82 scaled up by a factor of 10 in infrared and Brγ luminosity (Rieke et al. 1980) and molecular mass (Young & Scoville 1984). There is no obvious evidence for Seyfert activity. Rowan-Robinson & Crawford (1989) have estimated from a decomposition of its energy distribution that 78% of the luminosity can be attributed to the starburst, 17% to disk emission and at most 5% to a possible AGN contribution. Our upper limits of [Si VI] 1.96 μm/H_2 (1–0)$S(3)$ 1.957 μm <0.2 and [Si VI]/L_{IR} $<2 \times 10^{-6}$ are also a factor ≥ 25 smaller than measured for NGC 1068 (Oliva & Moorwood 1990) whose infrared luminosity is comparable and appears to comprise roughly equal contributions from starburst and Seyfert activity (Telesco et al. 1984). The effective temperature of the ionizing stars present, which depends primarily on their upper mass cutoff, is constrained by the observed He I 2.058 μm/Brγ ratios (Doyon, Puxley, & Joseph 1992). In the case of NGC 3256 the ratio we measured here is actually equal to the mean of two values measured by Doyon et al. on different positions of the galaxy and corresponds to an upper mass cutoff of ~ 30 $M_\odot$ under the various assumptions made in their model.

Starburst models which relate the bolometric luminosity to the emission rate of stellar Lyman continuum photons can also be used as a further test of the starburst nature of this galaxy and also to estimate the expected supernova rate which will be of particular interest below. The most convenient model for our present purpose is that for an extended starburst lasting $\sim 10^8$ yr due to Gehrz, Sramek, & Weedman (1983) who have tabulated the ratio of bolometric to Hα luminosity plus the supernova and star formation rates for various combinations of the upper and lower mass cutoffs and slopes of the initial mass function (IMF). A difficulty with this and all similar models which use hydrogen recombination lines to measure the emission rate of stellar Lyman continuum photons is the unknown fraction of these which are directly absorbed by dust within H II regions and therefore not available for photoionizing the gas. This is in addition to the problem of correcting the actually observed Hα emission for extinction. In the absence of more specific information we assume here that 2/3 of the Lyman continuum photons are absorbed by dust as found on average for Galactic H II regions from far-infrared and radio continuum measurements (Furniss, Jennings, & Moorwood 1974). The intrinsic Hα luminosities in the absence of dust can then be estimated from our dereddened Brγ luminosities using the case B recombination ratio Hα/Brγ = 100 which is virtually independent of density and temperature. Equating the infrared and bolometric luminosities finally yields $L/\mathrm{H}\alpha \sim 175$ which is in excellent agreement with the model prediction for an upper mass cutoff of 30 $M_\odot$ (consistent with the observed He I/Brγ ratio) a lower mass cutoff of 6 $M_\odot$ (lowest in this particular model) and an IMF slope ($m^{-\alpha}$) of $\alpha = 2.5$ (similar to our Galaxy).

Combined with the estimated absolute Hα luminosity derived from Brγ the model with these IMF parameters yields a star-formation rate of 20 $M_\odot$ yr^{-1} and a supernova rate of ~ 1.6 yr^{-1}. As the infrared and Brγ luminosities are dominated by the massive stars in the burst it should be noted that they are virtually insensitive to the lower mass cutoff. In estimating the above supernova rate, therefore, it has been implicitly assumed that the actual lower mass cutoff is below 6 $M_\odot$ and that all stars of this mass and higher explode as supernovae. The supernova rate can also be independently estimated from the nonthermal radio emission as follows. In our galaxy, the observed nonthermal 408 MHz radio luminosity and best estimate supernova rate of 0.023 yr^{-1} (Condon & Yin 1990) implies the following relationship between supernova rate (R_{sn}) and radio flux density at frequency ν for a galaxy with spectral index α and distance D (Mpc).

$$R_{sn} \sim S(\mathrm{mJy}) \times 8.7 \times 10^{-7} \times (\nu/1\ \mathrm{GHz})^{\alpha} \times D^2(\mathrm{Mpc}) . \quad (4.1)$$

For NGC 3256, with $S = 180$ mJy at 6 GHz, $\alpha \sim 1.38$ (Wright 1974) and $D = 37$ Mpc, we obtain $R_{sn} \sim 2$ yr^{-1} which is in excellent agreement with the 1.6 yr^{-1} derived from the starburst model. It should be noted, however, that this rate is a factor ~ 10 lower than estimated using the relationship given by Ulvestad (1982) which is based on the galactic Σ-D relationship and the Sedov solution for the adiabatic phase of radio emitting SNRs. This difference has been addressed by Condon & Yin who conclude that it can be largely attributed to the fact that the effective radio radiating lifetimes are longer than the $\sim 2 \times 10^4$ yr expected in this model.

The relevant observed and derived global properties of the starburst in NGC 3256 are summarized in Table 3. Of most interest is the fact that, although luminous and exhibiting a very high star-formation rate, its star-formation efficiency as measured by the ratio $L_{IR}/M_{H2} \sim 10$–20 (comparable to M82) is at the low end of the range found for starburst galaxies (Young & Scoville 1991). Its luminosity, however, is only a factor ~ 3 lower than those of the so-called Ultraluminous Infrared Galaxies which Sanders et al. (1988) have suggested may harbour quasars formed following intense starbursts triggered by the merging of two gas rich spiral galaxies. By analogy it could be assumed that somewhat lower luminosity starbursts would evolve into Seyferts. As we have concluded, based on our earlier discussion of the morphology, that the two nuclei have not yet merged NGC 3256 could still evolve into a Seyfert as the merger proceeds providing that the extended molecular gas is funnelled into the nucleus. Based on the dynamical mass in the central few kpc and assuming only a single stellar mass to characterize the starburst, however, Graham et al. (1984) showed that the kinetic energy supplied by supernovae exceeds GM^2/r implying that all of the gas could be swept out of the system. Using the subsequently mea-

TABLE 3

GLOBAL PROPERTIES OF NGC 4945 AND NGC 3256

Quantity	NGC 3256	NGC 4945
L_{IR} (10^{10} $L_\odot$)	30	2
M_{H_2} (10^8 $M_\odot$)	~170–300	~0.45–2.2
L_{IR}/M_{H_2}	~10–20	~90–450
Dynamical mass ($M_\odot$)	>5E10	~1E9
Lyc (10^{53} photons s^{-1})	~55	~1.2
SFR ($M_\odot$ yr^{-1})	~20	~0.5
R_{sn} (IR) yr^{-1}	~1.6	~0.03
R_{sn} (6 GHz) yr^{-1}	~2	~0.05

sured molecular gas mass and the supernova rates inferred above we also conclude that this condition can be met for a starburst duration exceeding 10^7 yr. On the other hand, the morphology of the [Fe II] and H_2 line emission does not provide clear evidence for a wind directed along the rotational axis although this may be attributable to its unfavourably low inclination. While the extension of the H_2 emission relative to Brγ in the SE, which corresponds roughly with our favoured position for the minor axis, could also be indicative of emission extending further out of the plane its spatial correlation with the spiral arm to the S of the nucleus suggests that this is probably not the case. Whereas there is enough energy to expel the gas therefore there is no obvious observational evidence that this is occurring and its ultimate fate is unclear.

4.1.2. *Origin of the Infrared Line Emission*

The most obvious mechanism for producing the Brγ emission in NGC 3256 is photoionization of H II regions by OB stars. This assumption is consistent both with the correspondence of its morphology with visible "hot spots" and the observed infrared luminosity as shown already above in the context of starburst models.

The spatial distribution of the [Fe II] emission is superficially similar to that of Brγ except that it is slightly more extended and does not exhibit such strongly pronounced peaks at the position of the visible "hot spots." This latter is not surprising as the iron should be in higher ionization stages than Fe^+ in H II regions ([Fe II] 1.64 μm/Brγ ~ 0.06 on the Trapezium region in Orion from the [Fe II] 1.26 μm/Pβ ratio measured by Lowe, Moorhead, & Wehlau 1979). Photodissociation regions are also unlikely to contribute significantly to the [Fe II] 1.64 μm emission. The model of Burton, Hollenbach & Tielens (1989) predicts a [Fe II] 26 μm line intensity of only ~3 times that of the H_2 (1–0) line and the [Fe II] 1.64 μm line is expected to be a factor ~1000 fainter. A morphology similar to that of the ionized gas is not entirely unexpected, however, if this emission is associated with SNRs whose progenitors are predominantly massive stars and which are strong [Fe II] emitters due to their large Fe^+ abundances resulting from grain destruction by moderately fast shocks and the absence of hard ionizing radiation. Theoretical predictions of [Fe II] 1.64 μm/Brγ ~ 20–70 (Shull & Draine 1987) have been confirmed observationally for Galactic and LMC remnants (Oliva, Moorwood, & Danziger 1989, 1990). The most luminous remnant detected so far, N49 in the LMC, emits [Fe II] 1.64 μm ~700 $L_\odot$ implying that ~10^{-3} of the canonical SN explosion energy of 10^{51} ergs is emitted in this line assuming a radiating lifetime of ~10^4 yr. For the estimated supernova rate of ~1.6 yr^{-1} for NGC 3256 and assuming the canonical energy release of 10^{51} ergs in a SN explosion the energy input rate is 5.2×10^{43} ergs s^{-1}. If a fraction 10^{-3} of this is reradiated in the [Fe II] 1.64 μm line then its expected luminosity is 1.4×10^7 $L_\odot$ or a factor of ~1.5 larger than observed. On purely energetic grounds, therefore, SNR's could account for all of the observed emission. Taking into account the spatial distribution and absence of line splitting it also appears most likely that the [Fe II] emission originates throughout the molecular complex. Assuming a cosmic abundance ratio (Fe/H ~ 6.5×10^{-6}) and that the bulk of the gas is molecular, the fraction f of the total Fe present required to radiate the observed [Fe II] 1.64 μm from a region of density n and temperature T is given by

$$f = 5 \times 10^{-19} L([\text{Fe II}])/j(n, T) \times M , \qquad (4.2)$$

where the line luminosity L and gas mass M are in solar units. The quantity j is the emissivity of the [Fe II] 1.64 μm line in ergs s^{-1} ion^{-1} whose dependence on temperature and density is shown in Figure 11 as computed for a 16 level ion using collision strengths and transition probabilities from Nussbaumer & Storey (1980, 1988). The observed upper limits on the [Fe II] 1.535/1.64 μm and 1.6/1.64 μm line ratios imply $n_e <$ 5000 cm^{-3} in the [Fe II] emitting regions (Oliva et al. 1990). Unfortunately, we have no temperature sensitive line ratios and the most plausible assumption we can make is that the [Fe II] lines arise in regions at T ~ 8000 K as found in Galactic supernova remnants and which is probably a characteristic temperature for partially ionized regions (Oliva et al. 1989). In this case $j \sim 10^{-17}$ ergs s^{-1} ion^{-1} and equation 4.2 yields $f \sim$ few $\times 10^{-5}$ i.e., only a very small fraction of the iron present would have to be shock heated and singly ionized in or at the surfaces of the molecular clouds to account for the observed emission. Using equation (4.2) it can also be shown that the lowest possible temperature in the [Fe II] emitting regions would be T ~ 1000 K, irrespective of density, even under the extreme and implausible assumption that all of the Fe in these galaxies is in the gas phase and singly ionized. There is thus a second compelling argument in addition to that based on the [Fe II]/H_2 ratio for believing that photodissociation regions cannot contribute significantly to the [Fe II] emission.

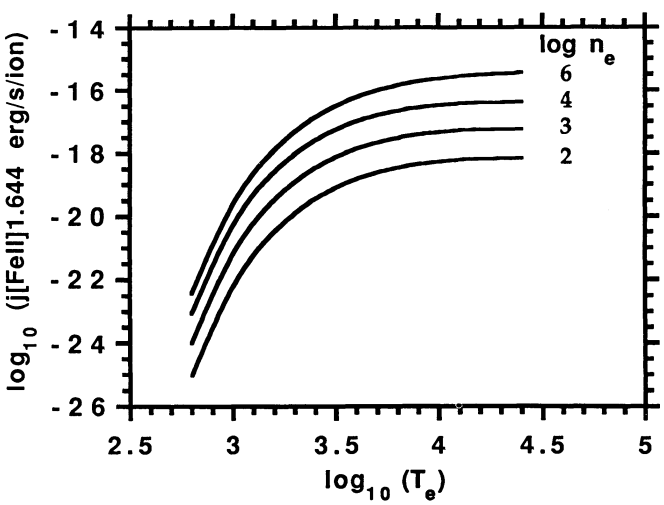

FIG. 11.—Emissivity of the [Fe II] 1.64 μm line in ergs s^{-1} ion^{-1} as a function of temperature and density.

Based on the (2–1)S(1)/(1–0)S(1) line ratio of 0.13 observed in the central region the H_2 emission appears to be thermally excited in gas at $\sim$2000 K (see also Moorwood & Oliva 1990). This emission does not arise in the [Fe II] emitting regions therefore and most probably arises from gas deeper in the molecular clouds which is heated by slow shocks and/or X-rays. At $T \sim 2000$ K the masses of H_2 required to account for the observed (1–0)S(1) line luminosities is only $\sim$7000 $M_\odot$, i.e., only a very small fraction of the total gas mass. Based on the models of Draine & Woods (1990a, b) a fraction 10^{-3} of the energy input from supernovae could be reradiated in the (1–0)S(1) line via direct shock and/or X-ray heating of surrounding molecular gas. Observational support for this has also been provided by partial mapping of the extended (1–0)S(1) line emission associated with the Galactic SNR RCW 103 which implies a value greater than 5×10^{-4} (Oliva, Moorwood, & Danziger 1990, and subsequent unpublished observations). In NGC 3256, therefore, the (1–0)S(1) line luminosity associated with SN/SNR could be as high as $\sim 2 \times 10^7$ $L_\odot$ or almost a factor of 5 larger than observed. In addition, there should also be some UV excited H_2 emission from high-density photodissociation regions associated with hot stars which, in the most favorable case (field strength, density, geometry) can exceed the Brγ emission (Puxley, Hawarden, & Mountain 1990; Moorwood & Oliva 1990; Mouri 1992) and hence could also account for all the observed H_2 luminosity. As already noted, however, the detailed spatial distribution of the (1–0)S(1) line emission does not convincingly correlate with that of either [Fe II] 1.64 μm or Brγ which we have presumed to be reliable tracers of hot stars and SN/SNRs. Given that these appear to be able to supply more than enough energy to excite the (1–0)S(1) line, however, we conclude that its morphology probably reflects more that of the molecular gas distribution or differences in the ages of the star forming regions, e.g., to the E and NW compared with the spiral arm to the S of the nucleus.

4.2. *NGC 4945*

4.2.1. *Starburst versus Seyfert Activity*

Evidence for the presence of both starburst and Seyfert activity in this galaxy has been reviewed in § 1.2. The large depth of the silicate absorption feature (Moorwood & Glass 1984); the lower limit of $\tau \geq 0.35$ at 100 μm deduced by Brock et al. (1988) (corresponding to $A_v > 175$ mag) and the column density $N_H \sim 10^{24.7}$ cm^{-2} deduced from the X-ray data by Iwasawa et al. (1993) also suggest that this is the most heavily obscured Seyfert nucleus known. Our failure to detect the coronal [Si VI] line, searched for specifically to test for the presence of Seyfert activity, may not be significant therefore. Although, normalized to the infrared luminosity, the upper limit on this line is a factor of 35 weaker than in NGC 1068 this difference could be accounted for if the extinction to the coronal line region exceeds $A_v \sim 50$ mag which appears to be likely.

As the detected infrared emission lines are all narrow and spatially extended they cannot arise predominantly in the nucleus itself. Using the Brγ luminosity corrected for the extinction derived from the Brγ/Brα ratio yields a ratio L_{IR}/Brγ which is a factor of 3 larger than NGC 3256 suggesting that a significant fraction of the infrared luminosity could be emitted by dust heated by the Seyfert nucleus. This would be qualitiatively consistent with the fact that most of the far-infrared emission arises from a region $\leq 12'' \times 9''$ (Brock et al. 1988) which is somewhat smaller than the $20'' \times 10''$ extent of the Brγ emission mapped here and which we assume delineates the starburst region. Even in X-rays the nucleus is obscured below $\sim$10 keV but Iwasawa et al. (1993) have estimated an intrinsic 2–10 keV luminosity of $L_X \sim 3 \times 10^{41}$ ergs s^{-1} by extrapolating the observed emission at higher energies of up to 30 keV assuming a constant spectral slope. This value can be compared with $L_X \sim 2$–4. 10^{43} ergs s^{-1} obtained in the same energy band by Koyama et al. (1989) from NGC 1068 whose infrared luminosity of 3×10^{11} $L_\odot$ appears to be equally shared between starburst and Seyfert components (Telesco et al. 1984). Assuming proportionality between X-ray and infrared luminosities would imply that only $\sim$15% of the infrared luminosity in NGC 4945 is associated with the Seyfert nucleus. The uncertainties are large however plus the extinction around 2 μm may also have been underestimated if it occurs in clumps (clouds) leading to an underestimate of the Brγ luminosity. The L_{IR}/Brγ ratio for the starburst component in NGC 4945 may not, therefore, be significantly higher than that observed for NGC 3256. The ratio He I (2.058)/Brγ = 0.62 $\pm$ 0.18 is somewhat higher and (because it is close to the saturation value) can only be used to establish an upper mass cutoff greater than 30 $M_\odot$ following Doyon et al. (1992). Using the same constraints on the IMF as for NGC 3256 the Gehrz et al. (1983) starburst model yields a star-formation rate of $\sim$0.5 $M_\odot$ yr^{-1} and a supernova rate of $\sim$0.035 yr^{-1} which is extremely close to the 0.05 yr^{-1} derived from the nonthermal radio emission (2 Jy at 6 GHz) using equation (4.1).

Global properties of NGC 4945 are summarized in Table 3 together with those for NGC 3256 for comparison. The $\sim 5 \times 10^7$ $M_\odot$ of H_2 in NGC 4945 derived by Whiteoak et al. (1990) from their CO observations is rather low and would imply a ratio $L_{IR}/M_{H_2} \sim 450$ which would be the highest observed in any galaxy (cf. Young & Scoville 1991). One possibility is that a large fraction of the molecular gas initially present may already have been funneled into a supermassive object responsible for the Seyfert activity. As noted already in in § 1.1, Bergman et al. (1992) deduce a mass about 5 times larger (scaling their quoted value to our adopted distance) which is consistent with Whiteoak et al. within their uncertainties but still only corresponds to about 15% of the dynamical mass within the region occupied by the molecular complex. A ratio $L_{IR}/M_{H_2} \sim 45$ could actually be closer to a realistic measure of the current star-formation efficiency therefore if we assume this larger molecular mass and that about half the infrared luminosity is associated with the active nucleus. This is, nevertheless, still larger than in NGC 3256 indicating that high star formation efficiency is not necessarily restricted to merger induced starbursts. As the ratio of dynamic mass to supernova rate is probably about the same in these two galaxies there is also no particular reason to believe that the gas will be more readily blown out of the merging system NGC 3256 than NGC 4945 and there is, in fact, more evidence for a starburst and/or AGN-driven wind in the latter.

4.2.2. *Origin of the Infrared Line Emission*

The fact that the Brγ emission is confined to a relatively thin disk in the plane of the galaxy and its luminosity is consistent with starburst models suggests that it originates in photoionized gas. Hot stars are also required to account for the large He I 2.06 μm/Brγ ratio. We do not, therefore, agree with the conclusion of Koornneef (1993) that NGC 4945 is a post star-

burst galaxy whose Brγ emission is predominantly shock excited. As [Fe II]/Brγ should be a factor of more than 100 larger in shocked compared with photoionized gas (see § 4.1.2) this idea is also not consistent with the fact that the observed ratio in NGC 4945 is almost the same as in NGC 3256.

The most striking feature of the infrared line maps (Fig. 8) is the roughly symmetrical extension of both the [Fe II] and H_2 emission relative to Brγ on both sides of the galactic plane. Figure 12 shows traces of the line surface brightnesses and ratios along a line running from SE to NW and passing through the nucleus. While all lines peak strongly on the nucleus it appears that the Brγ distribution may be slightly displaced and somewhat broader in the central region but cuts off much more sharply than the [Fe II] and H_2 lines whose spatial distributions are extremely similar and extend much further on both sides of the plane. At least away from the plane of the galaxy, therefore, these lines cannot be excited directly by the massive stars produced in the starburst. Rather, this morphology implies a contribution to these lines from a supernova-driven wind and/or the active nucleus. Evidence for the existence of a wind in the form of optical line splitting (Heckman et al. 1990) has already been cited and was attributed by these authors to the collective effects of SN before the X-ray confirmation of Seyfert activity. For an expansion velocity of only 100 km s^{-1} such a wind could extend to at least 1 kpc for a starburst 10^7 yr old. Adopting the same reasoning as for NGC 3256 the [Fe II] and H_2 line luminosities expected with the supernova rate of ~ 0.05 yr^{-1} deduced above would be $\sim 5 \times 10^5$ $L_\odot$ compared with the observed (extinction corrected) values of 3 and 4×10^5 $L_\odot$, respectively. Given the uncertainties, therefore, excitation of these lines by a supernova-driven wind cannot be excluded on energetic grounds. In addition to its larger L_{IR}/Brγ ratio, however, NGC 4945 also exhibits a factor of ~ 3 larger H_2 (1–0)S(1)/Brγ ratio compared with NGC 3256 which already exhibits one of the largest observed in starburst galaxies. It is also known from earlier surveys (Kawara, Nishida, & Gregory 1987; Moorwood & Oliva 1988) that the H_2 (1–0)S(1)/Brγ ratios tend to be somewhat larger in galaxies containing Seyfert nuclei compared with pure starbursters. As heating by X-rays associated with shocked gas now appears to be an important excitation mechanism for the H_2 emission in starburst regions this "excess" can be most naturally attributed to additional molecular gas heating by X-rays emitted by the active nucleus. Based on a SN rate of 0.05 yr^{-1} and assuming that 20% of their explosion energy is radiated in X-rays (Draine & Woods 1990b), the expected X-ray luminosity associated with SN is actually close to the nuclear X-ray luminosity of $\sim 3 \times 10^{41}$ ergs s^{-1}. Given the uncertainties in these estimates, therefore, it is not clear which source might dominate. Assuming that the nuclear X-rays are somewhat collimated along the rotational axis by a torus, which could be responsible for the high line of sight extinction, the morphology could also be similar in both cases. The starburst in NGC 3256, however, does not appear to lead to extended H_2 emission along the minor axis and the much larger (1–0)S(1)/Brγ ratio in NGC 4945 compared with NGC 3256 is also typical of the systematic difference found between composite starburst/Seyfert and starburst galaxies. We therefore propose that these differences can be attributed to the dominance of the Seyfert nucleus as a source of H_2 excitation. The similarity of the [Fe II] spatial distribution could also be accounted for if its extended component arises in gas which is partially ionized by X-rays (Mouri et al. 1993). Although the [Fe II] 1.64 μm/Brγ ratio is not enhanced relative to NGC 3256 the ratio in both galaxies is again above average for starburst galaxies (Moorwood & Oliva 1988). Relative to excitation by SNRs in the starburst region, enhancement of the H_2 emission by X-rays from the nucleus is also likely to be more pronounced than the increase in [Fe II] emission from the associated partially ionized gas where the depletion of Fe remains high in the absence of grain destruction.

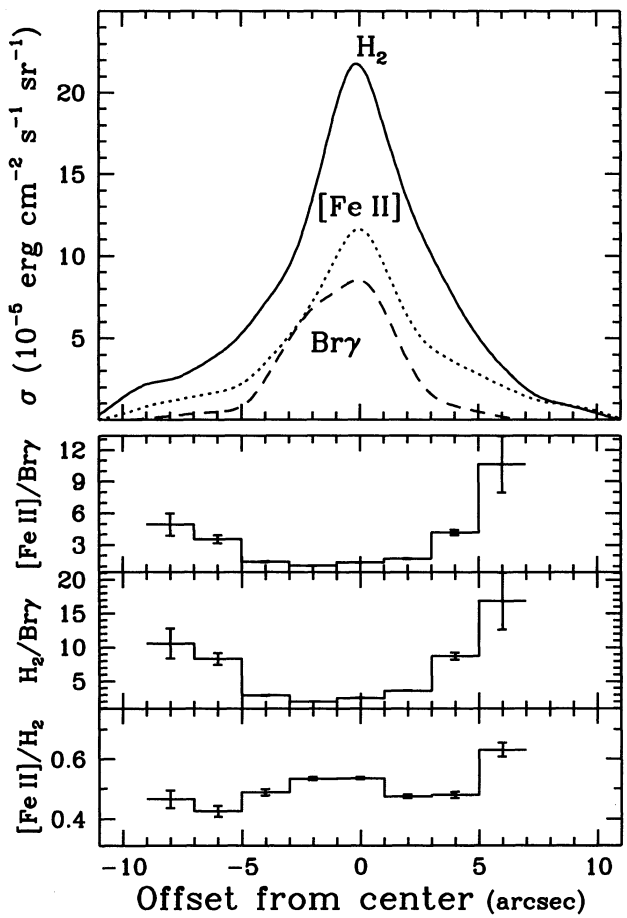

FIG. 12.—Traces of the surface brightness and ratios of the [Fe II] 1.64 μm, H_2 (1–0)S(1) and Brγ lines from SE to NW and passing through the nucleus of NGC 4945.

5. CONCLUSIONS

Infrared line emission mapped over ~ 4 kpc in the merging system NGC 3256 can be attributed to massive star formation. The Brγ emission arises in H II regions photoionized by OB stars whose upper mass cutoff is ~ 30 $M_\odot$; [Fe II] 1.64 μm is predominantly shock excited by supernova remnants while the H_2 (1–0)S(1) 2.121 μm line arises mostly in gas heated by stellar UV photons and X-rays produced by SN/SNRs. The H_2 emission is less peaked on the nucleus than the other lines and is more prominent on a newly discovered spiral arm and embedded source to the south of the nucleus which also appears in our K'(2.1 μm) image but is completely obscured by dust in the visible. We conclude that this source is probably the nucleus of the merging companion galaxy. Further evidence that the merger is not yet complete is provided by our K' image which

does not support earlier claims that the stellar light profile is already characteristic of a relaxed system. Although both the estimated star-formation ($\sim 20\ M_\odot\ yr^{-1}$) and supernova ($\sim 1.5\ yr^{-1}$) rates are high the star-formation efficiency in NGC 3256 is relatively low. The infrared line morphology does not indicate excitation by a starburst driven superwind or outflow/irradiation by an active nucleus and our search for [Si VI] 1.962 μm coronal line emission as evidence of visually obscured Seyfert activity proved negative.

In NGC 4945 the Brγ emission is mostly confined to a disk of diameter 380 pc and thickness ≤ 190 pc in the plane of the galaxy and can be attributed to photoionization by recently formed OB stars with masses of up to at least 30 $M_\odot$. While the star formation ($\sim 0.5\ M_\odot\ yr^{-1}$) and supernova ($\sim 0.05\ yr^{-1}$) rates are much lower than in NGC 3256 the star-formation efficiency is higher even if account is taken of the fact that up to half the observed infrared luminosity could be powered by the Seyfert nucleus. Our failure to detect coronal [Si VI] emission is consistent with this being the most heavily obscured Seyfert nucleus known. Relative to Brγ, which shows a very sharp cutoff on both sides of the galactic plane, the [Fe II] and H_2 (1–0)S(1) line emission is observed to extend a factor ~ 2 further in both directions and exhibit closely similar intensity profiles. The integrated H_2 (1–0)S(1)/Brγ ratio is a factor of ~ 3 larger than in NGC 3256 and [Fe II]/Brγ, although comparable with the ratio measured in NGC 3256, is also above average for starburst galaxies. We conclude that the [Fe II] and H_2 emission comprises a "starburst" component excited predominantly by SNRs (shock and X-ray, respectively) plus an additional "halo" component excited by X-rays from the nucleus (partial ionization and heating, respectively) which are partially collimated along the rotational axis. This phenomenon could provide a more general explanation for the enhanced [Fe II]/Brγ and H_2/Brγ ratios observed in composite starburst/Seyfert compared with pure starburst galaxies.

Overall, we conclude that the moderate luminosity, noninteracting, galaxy NGC 4945 shows some of the characteristics expected of a galaxy evolving from a starburster to a Seyfert whereas the highly luminous system NGC 3256 exhibits only extended and relatively low-efficiency star-formation activity and the merger is probably not yet sufficiently advanced to have formed/fuelled a supermassive object.

We are grateful to Reynier Peletier for useful discussions and for fitting the ellipses to our K' image of NGC 3256 and to Duncan Forbes for details of the recent radio observations showing a double nucleus in NGC 3256 in advance of publication.

REFERENCES

Allen, D. A., Norris, R. P., Meadows, V. S., & Roche, P. F. 1991, MNRAS, 248, 528
Baan, W. A. 1985, Nature, 315, 26
Bergman, P., Aalto, S., Black, J. H., & Rydbeck, G. 1992, A&A, 265, 403
Black, J. H., & van Dishoeck, E. F. 1987, ApJ, 322, 412
Brock, D., Joy, M., Lester, D. F., Harvey, P. M., & Ellis, H. B., Jr. 1988, ApJ, 329, 208
Burton, M., Hollenbach, D., & Tielens, A. G. G. M. 1989, in Infrared Spectroscopy in Astronomy, ed. B. H. Kaldeich (ESA SP-290), 141
Condon, J. J., Huang, Z.-P., Yin, Q. F., & Thuan, T. X. 1991, ApJ, 378, 65
Condon, J. J., & Yin, Q. F. 1990, ApJ, 357, 97
de Vaucouleurs, G., & de Vaucouleurs, A. 1961, MNRAS, 68, 69
de Vaucouleurs, G., de Vaucouleurs, A., & Corwin, H. G. 1976, Second Reference Catalogue of Bright Galaxies (Austin: Univ. Texas Press)
Doyon, R., Puxley, P. J., & Joseph, R. D. 1992, ApJ, 397, 117
dos Santos, P. M., & Lepine, J. R. D. 1979, Nature, 278, 34
Draine, B. T., & Woods, D. T. 1990a, ApJ, 363, 464
———. 1990b, ApJ, 383, 621
Feast, M. W., & Robertson, B. S. C. 1978, MNRAS, 185, 31
Furniss, I., Jennings, R. E., & Moorwood, A. F. M. 1974, in H II Regions and the Galactic Center, ESRO SP-105, ed. A. F. M. Moorwood (Noordwijk: ESTEC), 61
Gehrz, R. D., Sramek, R. A., & Weedman, D. W. 1983, ApJ, 267, 551
Glass, I. S., & Moorwood, A. F. M. 1985, MNRAS, 214, 429
Graham, J. R., Wright, G. S., Meikle, W. P. S., Joseph, R. D., & Bode, M. F. 1984, Nature, 310, 213
Graham, J. R., Wright, G. S., Joseph, R. D., Frogel, J. A., Phillips, M. M., & Meikle, W. P. S. 1987, in Star Formation in Galaxies, ed. C. J. Lonsdale Persson (NASA CP-2466), 517
Harnett, J. I., Haynes, R. F., Klein, U., & Wielebinski, R. 1989, 216, 39
Heckman, T. M., Armus, L., & Miley, G. K. 1990, ApJS, 74, 833
Iwasawa, K., Koyama, K., Awaki, H., Kunieda, H., Makishima, T., Tsuru, T., Ohashi, T., & Nakai, N. 1993, ApJ, 409, 155
Kawara, K., Nishida, M., & Gregory, B. 1987, ApJ, 321, L35
———. 1989, ApJ, 342, L55
Koornneef, J. 1993, ApJ, 403, 581
Koyama, K., Inoue, H., Tanaka, Y., Awaki, H., Takano, S., Ohashi, T., Matsuoka, M. 1989, PASJ, 41, 731
Krügel, E., Tutukov, A., & Loose, H. 1983, A&A, 124, 89
Landini, M., Natta, A., Oliva, E., Salinari, P., Moorwood, A. F. M. 1984, A&A, 134, 284
Lauberts, A., Bergvall, N. A. S., Ekman, A. B. G., & Westerlund, B. E. 1978, A&AS, 35, 55
Lonsdale, C. J., Lonsdale, C. J., & Smith, H. E. 1992, ApJ, 391, 629
Lowe, R. P., Moorhead, J. M., & Wehlau, W. H. 1979, ApJ, 228, 191
Moorwood, A. F. M. 1986, A&A, 166, 4
Moorwood, A. F. M., & Glass, I. S. 1984, A&A, 135, 281
Moorwood, A. F. M., & Oliva, E. 1988, A&A, 203, 278
Moorwood, A. F. M., & Oliva, E. 1989, in IAU Symp. 134, Active Galactic Nuclei, ed. D. E. Osterbrock & J. S. Miller (Dordrecht: Reidel), 365
———. 1990, A&A, 239, 78
———. 1991, ESO Messenger, 63, 57
———. 1993a, in ASP Conf. Ser. 41, Astronomical Infrared Spectroscopy ed. S. Kwok, (San Francisco: ASP), 305
———. 1993b, Infrared Phys. Eng., in press
Moorwood, A. F. M., & Origlia, L. 1990, in ASP Conf. Ser. 14, Astrophysics with Infrared Arrays, ed. R. Elston (San Francisco: ASP), 85
Moorwood, A. F. M., Moneti, A., & Gredel, R. 1991, ESO Messenger, 63, 77
Moorwood, A. F. M., et al. 1992, ESO Messenger, 69, 61
Mouri, H. 1992, MNRAS, 257, 433
Mouri, H., Kawara, K., & Taniguchi, Y. 1993, ApJ, 406, 52
Nakai, N. 1989, PASJ, 41, 1107
Norris, R. P., & Forbes, D. A. 1994, in preparation
Nussbaumer, H., & Storey, P. J. 1980, A&A, 89, 308
———. 1988, A&A, 193, 327
Oliva, E., & Moorwood, A. F. M. 1990, ApJ, 348, L5
Oliva, E., Moorwood, A. F. M., & Danziger, I. J. 1989, A&A, 214, 307
———. 1990, A&A, 240, 453
Oliva, E., & Origlia, L. 1992, A&A, 254, 466
Puxley, P. J., Hawarden, T. G., & Mountain, C. M. 1990, MNRAS, 364, 77
Rice, G. H., Lonsdale, C. J., Soifer, B. T., Neugebauer, G., Kopan, E. L., Lloyd, L. A., de Jong, T., & Habing, H. J. 1988, ApJS, 68, 91
Rieke, G. H. 1988, ApJ, 331, L5
Rieke, G. H., Lebofsky, M. J., Thompson, R. I., Low, F. J., & Tokunaga, A. T. 1980, ApJ, 238, 24
Rowan-Robinson, M., & Crawford, J. 1989, MNRAS, 238, 523
Sanders, D. B., Soifer, B. T., Elias, J. H., Madore, B. F., Matthews, K., Neugebauer, G., & Scoville, N. Z. 1988, ApJ, 325, 74
Sargent, A. I., Sanders, D. B., & Phillips, T. G. 1989, ApJ, 346, L9
Schweizer, F. 1983, in IAU Symp. 100, ed. E. Athenassoula (Dordrecht: Reidel), 319
———. 1986, Science, 231, 227
Shull, J. M., & Draine, B. T. 1987, in Interstellar Processes, ed. D. J. Hollenbach & H. A. Thronson, Jr. (Dordrecht: Reidel), 283
Telesco, C. M., Becklin, E. E., Wynn-Williams, C. G., & Harper, D. A. 1984, ApJ, 282, 427
Toomre, A., & Toomre, J. 1972, ApJ, 178, 623
Ulvestad, J. S. 1982, ApJ, 259, 96
Weedman, D. W., Feldman, F. R., Balzano, V. A., & Ramsey, L. W. 1981, ApJ, 248, 105
Whiteoak, J. B., Dahlem, M., Wielebinski, R., & Harnett, J. I. 1990, A&A, 231, 25
Whiteoak, J. B., & Wilson, W. E. 1990, MNRAS, 245, 665
Wright, A. E. 1974, MNRAS, 167, 251
Young, J. S., & Scoville, N. Z. 1984, ApJ, 287, 153
———. 1991, ARA&A, 29, 581